EXPERIMENTAL AND FINITE ELEMENT ANALYSIS OF BENDING TEST OF *GIGANTOCHLOA ATROVIOLACEA* (WULUNG BAMBOO): LINEAR-ISOTROPIC MATERIAL USING BENDING PROPERTIES

Ditya Ramadhanti, Inggar Septhia Irawati[*], Angga Fajar Setiawan

Department of Environmental and Civil Engineering, Faculty of Engineering, Universitas Gadjah Mada, Jalan Grafika 2, Yogyakarta, Indonesia
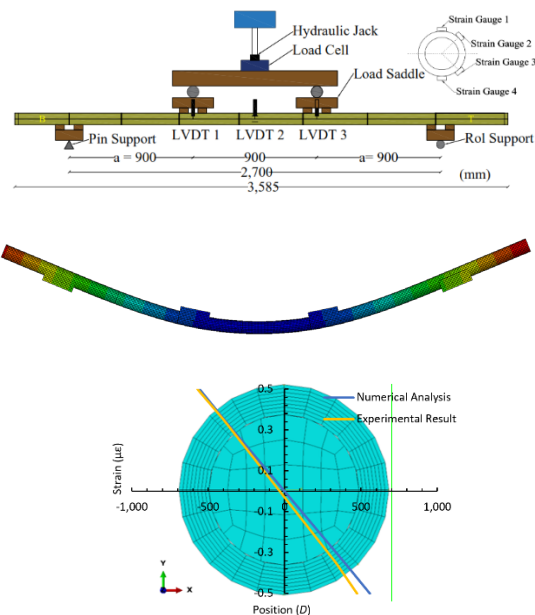
Abstract

Predicting the flexural behavior of bamboo beams is challenging due to their complex shape and disparate material properties. This study evaluates the accuracy of numerical analysis in predicting bamboo flexural behavior, utilizing a homogeneous bamboo diameter approach and applying the flexural modulus of elasticity property. Wulung bamboo was used for the bending experiment, following ISO 22157:2019. Finite element analysis was conducted using Abaqus CAE software. The numerical results were compared with experimental results including deflection, neutral axis position, strain, and stress. Results indicate that numerical modeling of a bamboo beam can predict Wulung bamboo's linear deformation, with a 2.03% discrepancy. The neutral axis from numerical analysis deviates by 3.43 mm and 6.69 mm above experimental measures under elastic and ultimate loads, respectively. The numerical analysis bamboo beam model shows closer results in predicting the compressive strain than predicting the tensile strain of a bamboo beam. The difference in maximal compressive strain on the topmost surface between numerical analysis and experimental results ranges from 1.92% to 15.1%. The difference in maximal tensile strain on the bottommost surface between numerical analysis and experimental results ranges between 16.1% and 24.3 %. The maximum normal stress ratio to modulus of rupture is 0.995.

Keywords: Wulung bamboo, flexural test, finite element analysis, prismatic isotropic linear, bending properties

1.0 INTRODUCTION

Indonesia is a tropical country that has many types of plants, one of which is bamboo. The strength of bamboo is ten times stronger than traditional wood [1]. As a result, bamboo has great potential to be used as a construction material. So far, there have been several implementations of bamboo in the construction field, such as bamboo used for soil improvement, foundation poles, sheet walls, and scaffolding [2, 3].

There are several mechanical properties of bamboo, such as tensile and compressive strength parallel to the grain; tensile and compressive strength perpendicular to the grain; modulus of rupture known as flexural strength; and shear strength, which are used for designing bamboo structure [4]. Those properties

are obtained by laboratory testing conducted according to ISO 22157:2019. The selection of mechanical properties used for designing depends on the type of loading subjected to the bamboo culm.

The mechanical properties of bamboo are influenced by its physical properties, one of which is specific gravity [5]. Bamboo has a specific gravity of about $0.55 - 0.75$ kg/cm^2 [5]. The specific gravity value of bamboo between the internode and the node is different. In the node section, the number of vessels is less, the fiber length is shorter than in the internode section, and the diameter of parenchyma cells is more expansive than in the internode section [6, 7]. Thus, the specific gravity of the node is lower than that of the internode.

Various studies mention that the influence of geometry factors, position along the bamboo culm, and fiber orientation

results in different values of bamboo mechanical properties [6, 8]. Previous research results conducted by Chaowana *et al.*, (2021), show that *D.asper* bamboo has the highest resistance to ultimate load due to its largest diameter (with a range of 10-12 cm) compared to *D.sericus*, *D. membranaceus*, *Th. oliveri*, and *Ph. Makinoi* [6]. Oka *et al.*, (2014), mentioned that the shear, compressive, and tensile strength parallSel and perpendicular to grain at the node and internode of Wulung bamboo increased from bottom to top [8]. Candelaria *et al.*, (2019), mentioned in their research result that the tensile elastic modulus parallel to the grain of Kauayan Tinik bamboo is higher than that in the perpendicular direction [9]. Suriani (2020) found that Betung bamboo has a higher compressive strength parallel to grain than that in a perpendicular direction. Bamboo has different flexural, tensile, and compressive elastic moduli [10]. According to Siopongco and Munandar (1987) bamboo has a tensile modulus of elasticity parallel to the fibers ranging from 8,728 to 31,381 MPa, a compressive modulus of elasticity ranging from 5,590 to 21,182 MPa, and a flexural modulus of around 9,708 MPa [11]. Bamboo is also classified as a naturally functionally graded material (FGM) since the fiber volume increases radially from the inside to the outside of the bamboo culm surface [12]. The FGM structure of bamboo significantly affects its mechanical properties, one of which is tensile strength. The outer surface of bamboo with high fiber density has a higher tensile strength than the inner region with low fiber density [13]. The different geometric factors, the different strengths (in tensile, compressive, and flexural loading), and the natural FGM properties of bamboo are often not considered in designing bamboo structures as construction materials, especially bamboo under flexural load [4].

The complex shape and diverse material properties pose challenges in predicting the bending behavior of bamboo beams. However, in the bamboo beam design calculations stated in the ISO 22156:2021 bamboo structural design code, bamboo's geometric shape and material properties are simplified. The cross-sectional dimensions used in the design are the average cross-sectional dimensions of the top and bottom of the bamboo culm. The material properties of bamboo are assumed to be a homogeneous isotropic material, where stress and strain have the same value in all directions [4].

Theoretically, when a bamboo beam is laterally loaded, flexural stress-strain occurs in the direction parallel to its longitudinal axis, known as normal stress. However, the ISO 22156:2021 bamboo structural design code predicts the flexural behavior of the bamboo beam under elastic conditions by using the flexural mechanical properties, i.e., the modulus of elasticity and modulus of rupture [4]. Considering that the bending, compressive, and tensile elastic moduli of bamboo are different, the question arises as to whether the approach taken using bending strength and flexural elastic modulus in the analysis of bamboo beams can represent the flexural behavior of bamboo beams, in terms of deformation, neutral axis position, normal tensile and compressive strain as well as normal tensile and compressive stress.

Numerical research to obtain the answer to the above question has not been conducted [9, 14, 15, 16]. Candelaria *et al.*, (2019), analyzed the flexural behavior of bamboo using compressive and tensile properties to obtain the deformation and stress [9]. They modeled bamboo as an isotropic and orthotropic material. However, the model is not hollow bamboo beams but bamboo split with a rectangular cross-section. Irawati

et al., (2020), conducted a 1D numerical model of a hollow cylindrical cross-section bamboo beam by applying SAP2000 to predict the maximum lateral load that the bamboo beam can safely support by separately assigning three bending properties obtained from three different methods, i.e., average method, ISO 22156 method, and *MoE-MoR* relation method in three of 1D bamboo modeling [14]. Due to using a 1D model, the stress-strain of the bamboo beam has not been obtained. Ramful *et al.*, (2020), conducted a numerical study of bamboo to investigate the fracture mechanisms of bamboo subjected to bending, compression, torsion, and shear by assuming bamboo is a transversely isotropic material [15]. The model dimension has not been assigned in the structural dimension. The model only consisted of one internode part and a maximum of two node parts. Bamboo is assumed to be a non-linear isotropic material, and the research result is still limited to comparing the load-deflection curve from numerical and experimental studies.

Considering that it is crucial to identify the differences in the flexural behavior of bamboo beams analyzed using bending properties towards that obtained from the experimental study, this study aims to investigate the accuracy of the flexural behavior of bamboo beams resulting from numerical analysis and experiment. Hence, experimental and numerical studies are conducted. A four-point bending test of Wulung bamboo is conducted based on ISO 22157:2019. The ISO 22157:2019 standard was chosen because the Indonesia standard design for bamboo structures has not been available [17, 18, 19].

Wulung bamboo (*Gigantochloa atroviolacea*) is used in this research because it is one of Indonesia's bamboo species that has great potential to be applied to structural elements [20]. Wulung bamboo is used as a structural material for community center buildings in Pakuncen, Yogyakarta, Indonesia [21]. Due to Wulung bamboo' potential, Awaludin and Andriani (2014) researched the performance of bolted Wulung bamboo joints using Fiber Reinforced Plastic (FRP) [22]. Taufani and Nugroho (2014) proposed elementary school building designs using Wulung bamboo [23].

In this research, the flexural modulus of elasticity obtained from the bending test is applied as material properties of 3D bamboo modeling. Numerical modeling of 3D bamboo beams is developed by using Abaqus. Following the approach used by ISO 22156:2021, bamboo is assumed to be a linear isotropic material and the average dimensions of the top and bottom part of bamboo are used as the diameter of the bamboo beam model. The geometry of the bamboo model is adjusted to the bamboo specimen geometry and a bamboo bending test arrangement, such as bamboo dimension, node position, span, and loading position. Then, the deflection, tensile strain, and compressive strain from the numerical modeling will be compared to that

Note :
⊙ : Internode ▢: Node T: Top M: Middle B: Bottom (mm)
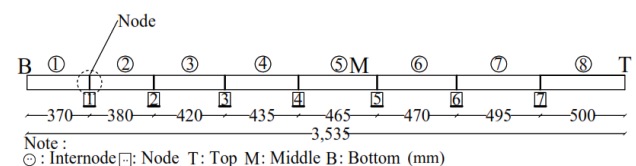
Figure 1 The specimen length
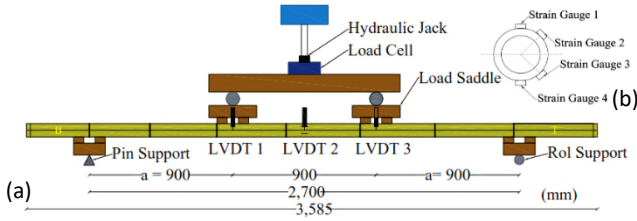
Figure 2 (a) The schematic of the four-point bending test as ISO 22157:2019; (b) The strain gauge location at mid-span

from the experimental results. Besides that, the maximum and the minimum normal stress obtained from numerical analysis when the bamboo was subjected to ultimate lateral load will be compared to the modulus of rupture (*MoR*) obtained from the experiment.

2.0 METHODOLOGY

2.1 Experimental Method

2.1.1 Material

The material used in this research is Wulung bamboo culm (*Gigantochloa atroviolacea*) from Seyegan District, Sleman Regency, Yogyakarta, Indonesia. The bamboo culm has been treated with 0.2% deltamethrin utilizing the VSD (Vertical Soak Diffusion) method. Bamboo specimens consist of internode and node sections. The number of nodes is 7, and the number of internodes is 8 (Figure 1). Figure 1 shows that the internode length along the bamboo culm varies. The length increases from the bottom to the top. The bamboo culm diameter at the bottom, center, and top parts are 86.3 mm; 84.8 mm; and 86.2 mm, respectively. The average bamboo culm diameter is 85,76 mm. The bamboo wall thickness at the bottom and top of the bamboo culm is 14.3 mm and 10.10 mm, respectively. The average bamboo wall thickness is 12.2 mm. Node thickness is 5 mm. ISO 22157:2019 [24] requires a bending specimen length of 30D. Thus, a bamboo specimen length of 3,585 mm is used.

2.1.2 Flexural Test

Flexural testing of bamboo beams was conducted following ISO 22157:2019. The four-point bending test setup can be seen in Figure 2a. Figure 2 shows that the two supports are placed precisely at the node. Since ISO 22157 requires the shear span *a* (Figure 2a), to be equal, placing the lateral load exactly at the node is difficult. The load can only be adjusted to be located as close to the node.

A flexural test was conducted using a 10-ton bending test machine. To measure displacement, LVDT 1 and 3 were installed at 1/3 span from the right and left supports, while LVDT 2 was installed at the center of the span. Four strain gauges were installed at the center of the span to measure strain, denoted as SG-1, SG-2, SG-3, and SG-4 for strain gauges 1, strain gauge 2, strain gauge 3, and strain gauge 4, respectively (Figure 2b). The strain gauges SG-1, SG-2, SG-3, and SG-4 were located at 0.5 D; 0.35 D; -0.35 D; and -0.5 D; respectively. The load, displacement, and strain occurring during loading were recorded. The bending

moment *M*, modulus of elasticity *MoE*, and modulus of rupture *MoR* were calculated by using Equations (1), (2), and (3), respectively. *P* is the applied lateral load; *a* is the length of the shear region that is equal to 1/3 of the span length; *D* is the average diameter of the bamboo beam; I_B is the moment of inertia; P_{20} and P_{60} are the loads at 20% and 60% of the ultimate load; Δ_{20} and Δ_{60} are the vertical deflection at midspan occurred at loading P_{20} and P_{60}, *L* is the bamboo span length; P_{ult} is the ultimate load.

$$M = \frac{Pa}{2} \ (MPa) \tag{1}$$

$$MoE = \frac{(P_{60}-P_{20})a(3L^2-4a^2)}{48(\Delta_{60}-\Delta_{20})I_B} \ (MPa) \tag{2}$$

$$MoR = \frac{16P_{ult}aD}{\pi(D^4-(D-2t)^4)} \ (MPa) \tag{3}$$

2.2 Numerical Analysis

2.2.1 Linear Isotropic Constitutive Equation

Numerical analysis was performed by creating a 3D model. The solid element type is used in this study. Bamboo is assumed to be an isotropic linear elastic material. The linear elastic condition makes the stress dependent on the deformation so that the stress is a function of the strain, as written in Equation 5 [25]. σ_{ij} is the stress vector, ε_{kl} is the elastic strain vector, and F_{ij} is the material stiffness matrix. The stress and strain relationship of linear isotropic materials can be seen in Equation 6 [26]. *E* is the elastic modulus, *v* is Poisson's ratio, and *G* is the shear modulus. *G* is calculated by using Equation 7. Linear elastic materials must meet the Drucker stability. The stability criteria of the above equation are *E*>0, *G*>0, and -1<*v*<0.5 [26].

$$\sigma_{ij} = F_{ij}(\varepsilon_{kl}) \tag{5}$$

$$\begin{Bmatrix} \varepsilon_{11} \\ \varepsilon_{22} \\ \varepsilon_{33} \\ \gamma_{12} \\ \gamma_{13} \\ \gamma_{23} \end{Bmatrix} = \begin{bmatrix} 1/E & -v/E & -v/E & 0 & 0 & 0 \\ -v/E & 1/E & -v/E & 0 & 0 & 0 \\ -v/E & -v/E & 1/E & 0 & 0 & 0 \\ 0 & 0 & 0 & 1/G & 0 & 0 \\ 0 & 0 & 0 & 0 & 1/G & 0 \\ 0 & 0 & 0 & 0 & 0 & 1/G \end{bmatrix} \begin{Bmatrix} \sigma_{11} \\ \sigma_{22} \\ \sigma_{33} \\ \sigma_{12} \\ \sigma_{13} \\ \sigma_{23} \end{Bmatrix} \tag{6}$$

$$G = E/2(1+v) \tag{7}$$

2.2.2 Modeling of Bamboo

The numerical modeling of bamboo beams in this study used the commercial finite element software with Abaqus CAE. The bamboo beam was modeled as a hollow circular prismatic beam. The bamboo beam model's dimensions were defined using the average diameter and average thickness data from the bending specimen measurements [4]. The outer diameter and inner diameter of the bamboo beam model were 85.77 mm and 61.36 mm, respectively. The node bamboo of 5 mm thickness was assigned in the model and located by referring to the node position of the bamboo specimen, as shown in Figure 1. The internode length, support, and load position in the 3D model

(Figure 3a) were defined the same as those in the bending test specimen (Figure 2a).
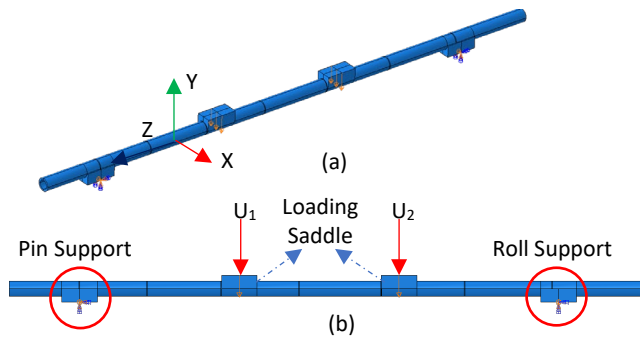
Figure 3 (a) The geometry modeling of Wulung bamboo beams; (b) The pin support, roller support, loading saddle, and the displacement control position in the modeling
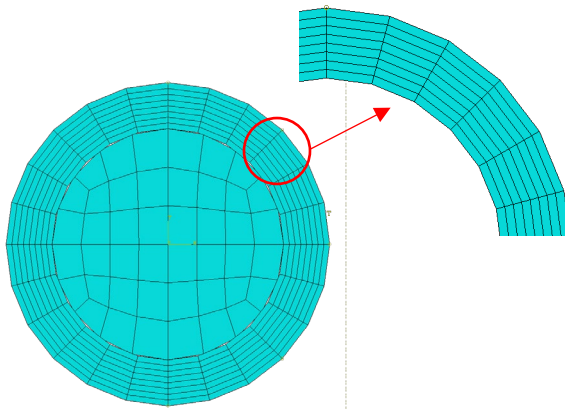
Figure 4 The meshing element of the bamboo wall section and bamboo node

The internode and node parts of the bamboo beam model were modeled as a hexahedral solid element. Then, the wall section of the bamboo beam model was divided into 8 layers in a radial direction (Figure 4). An 8-node linear continuum 3D element with reduced integration, C3D8R, was used as the base element. The direction of the local cartesian coordinate system was the same as that of the global cartesian coordinate system, as shown in Figure 3a. The Abaqus software defined the local cartesian coordinates using the material orientation function. The contact surfaces between the outer surface of the node and the inner surface of the internode bamboo beam model were tied together using a constraint tie. The contact surface of the load saddle, pin support saddle, and roller support saddle to the outer surface of the bamboo is defined as surface-to-surface contact interaction, each of which has a different friction coefficient value, i.e., 0.1; 0.3; and frictionless, respectively. Pin and roller support are defined as boundary conditions, as shown in Figure 3b.

Based on Equation 6, the mechanical properties required for numerical analysis are the modulus of elasticity and Poisson's ratio, as bamboo is assumed as an isotropic elastic linear material. The modulus of elasticity of 17,562.7 MPa is defined based on the result of the four-point bending test in this study. Poisson's ratio of 0.3 is defined based on the literature [15]. The

static loading on the bamboo model was assigned by using displacement control. The vertical displacement load, whose
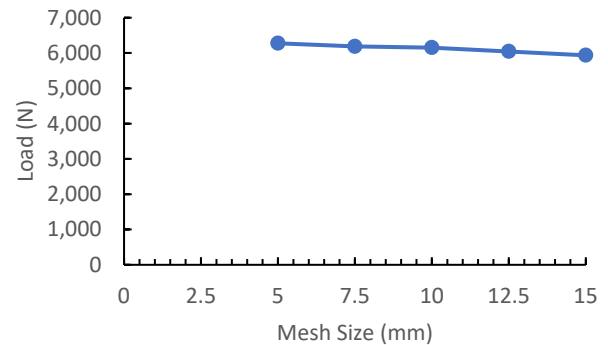
Figure 5 The convergence test curve

Table 1 The four-point bending test result and mechanical properties of bamboo.

$P_{elastic\ limit}$	4,750	N
P_{ult}	5,125	N
$\Delta_{elastic\ limit}$	48.475	mm
Δ_{Pult}	64	mm
MoE	17,562.7	MPa
MoR	50.4	MPa

value is obtained from the maximum displacement value of flexural testing, is applied as a boundary condition. The displacement load is positioned on each load saddle as a set of lines with a geometric type. The load saddle location (U_1 and U_2) can be seen in Figure 3b.

The mesh convergence test on the cross-section of the bamboo beam model was carried out using mesh size in the range of 5 to 15 mm on both the bamboo wall part and the bamboo node part. The convergence test results show that using a 10 mm mesh size produces the desired convergence rate, as shown in Figure 5. After the numerical analysis, the numerical modeling results are compared with the experimental results.

3.0 RESULTS AND DISCUSSION

3.1 Experimental Result

3.1.1 Load-Deflection Curve

The load-deflection curve resulting from the flexural test can be seen in Figure 6a. Observing the load-deflection curve, the mid-span deflection (LVDT 2) is greater than the deflection at 1/3 span (LVDT 1 and LVDT 3). The sloping graph of LVDT 2 indicates this compared to that of LVDT 1 and LVDT 3. Figure 6a shows that the bamboo behaves linearly until the load reaches 93% of the ultimate load, P_{ult}. After that, the bamboo behaves non-linearly until it reaches the ultimate load. Then, the load drops, but the deflection simultaneously increases.

The load and midspan deflection at the elastic limit are 4,750 N and 48.475 mm, respectively, as shown in Figure 6b. The figure

shows that the ultimate load P_{ult} and deflection when ultimate load occurred Δ_{Pult} are 5,125 N and 64 mm, respectively. *MoE* and *MoR* are obtained using Equations 2 and 3, *i.e.*, 17,562.7 MPa and 50.4 MPa, respectively. The flexural test results are summarized in Table 1.

3.1.2 Load-Strain Curve

The load-strain curve can be seen in Figure 7. The position of the strain gauges SG-1, SG-2, SG-3, and SG-4 can be seen in Figure 2b. The strain gauge 1 is located at the topmost surface of the bamboo beam, so it measures the maximum compressive strain. Strain gauge 4 is located on the bamboo's bottommost surface, so it measures maximum tensile strain. The strain value at each strain gauge occurred when the elastic limit and ultimate load reach can be seen in Table 2. The load-strain curve shows linear behavior until the load reaches 93% of the ultimate load P_{ult}.

According to the strain pattern in Figure 7, at the equal load, the compressive strain on strain gauge SG-1 is higher than that on strain gauge SG-2, while the tensile strain on strain gauge SG-4 is higher than that on strain gauge SG-3. The slope of the load-strain curve in the tensile region is not the same as that in

Table 2 The elastic load and ultimate load values

SG	$\varepsilon_{P\,elastic\,limit}$ (μɛ)	ε_{Pult} (μɛ)
SG-1	-2,700	-3,365
SG-2	-1,925	-2,615
SG-3	1,500	1,670
SG-4	2,130	2,460

(a)

(b)
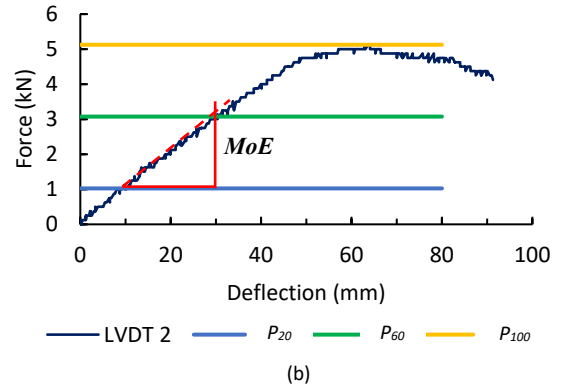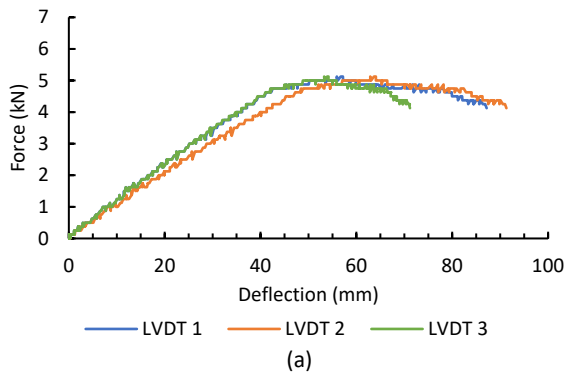
Figure 6 (a) The load-deflection curve of flexural test results, (b) The load-deflection curve of LVDT 2 and defining elastic modulus
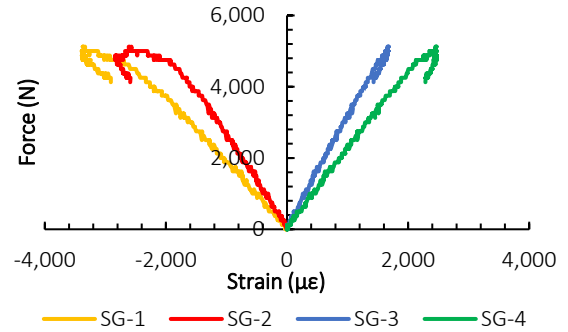
Figure 7 The strain-force curve of SG-1 to SG-4
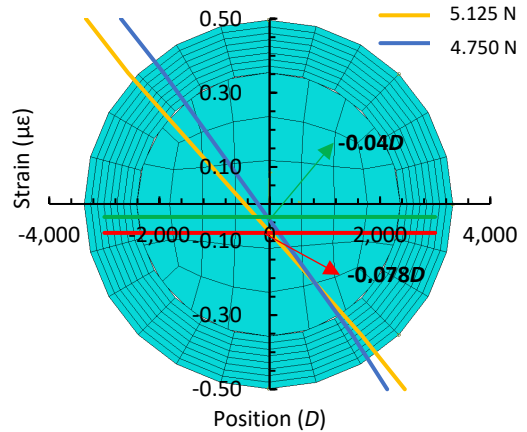
Figure 8 Strain and neutral axis plot of $P_{elastic}$ and P_{ult}

the compressive region. As a result, the neutral axis is not located at half the diameter of the bamboo culm cross-section. The neutral axis lies between the strain gauge SG-2 and SG-3.

The strain distribution along the beam's cross-section when the elastic limit and the ultimate load occur can be seen in Figure 8. Figure 8 also depicts the neutral axis position of the cross-section located in the midspan beam in the two loading stages, *i.e.*, elastic limit loading and ultimate loading. The figure shows that the neutral axis is located at -0.04 of the bamboo diameter

measured from the center point of the bamboo section when the elastic limit load is reached. When the load reaches the ultimate load, the neutral axis shifts to -0.078 of the bamboo diameter. It depicts that the neutral axis position changes with every change in load. This research result matches the previous research results conducted by Li *et al*., 2016 and Abzarih *et al*, 2022 [27, 16].

3.2 Numerical Result and Analysis

3.2.1 Load-displacement Curve

The deformed bamboo shape obtained from Abaqus CAE can be seen in Figure 9, where the maximum deflection occurs at mid-span, shown in a blue zone. The comparison of the load-displacement curve obtained from the experiment, theoretical analysis, and numerical analysis can be seen in Figure 10. It can be seen that the load-deflection curve below the elastic limit obtained from the experiment is very close to that obtained from theoretical analysis. This is because the theoretical deflection Δ is calculated using Equation 2, while the flexural elastic modulus *MoE* stated in Equation 2 is obtained from the experiment. Based on Figure 10, the numerical and experimental loading reaches 4,654 N and 4,776 N, respectively, when the midspan deflection reaches the plastic limit deflection (48.475 mm). The loading comparison when the experimental elastic limit deflection occurred is clearly shown in Table 3. It shows that the maximum difference between the load obtained from numerical analysis and the load obtained from the experiment is 2.03%. It means that numerical analysis can predict the load-deflection curve well at the loading stage until the load reaches the elastic limit. Previous research conducted by Candelaria et al., (2019), showed that the average error of the numerical analysis result using an isotropic material assumption compared to the four-point bending test results of the bamboo split was 19.26% [9]. Figure 10 shows that the load-displacement curve obtained from numerical differs from that resulted from the experiment after the load increased above the elastic limit load.

Table 3 The load value and deflection at the elastic limit of each method

Elastic Limit	NA* (a)	Theoretical (b)	Experiment (c)	Differences		
				(a/b)	(a/c)	(b/c)
P (N)	4,654	4,776	4,750	0.97	0.98	1.01
δ (mm)	48.475	48.475	48.475	-	-	-

*NA = Numerical Analysis

Figure 9 The deformed shape of bamboo culm under four-point bending test (displacement)
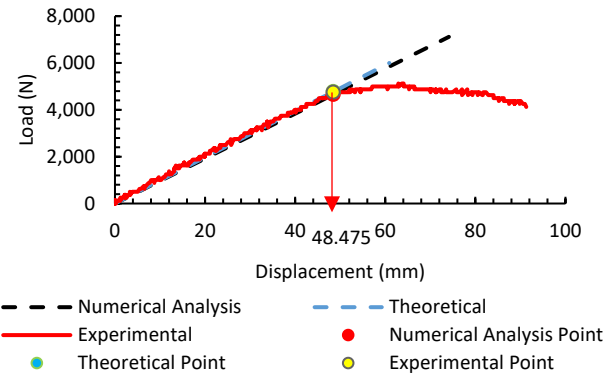
Figure 10 The load-displacement curve obtained from between numerical analysis, experiment, and theoretical analysis
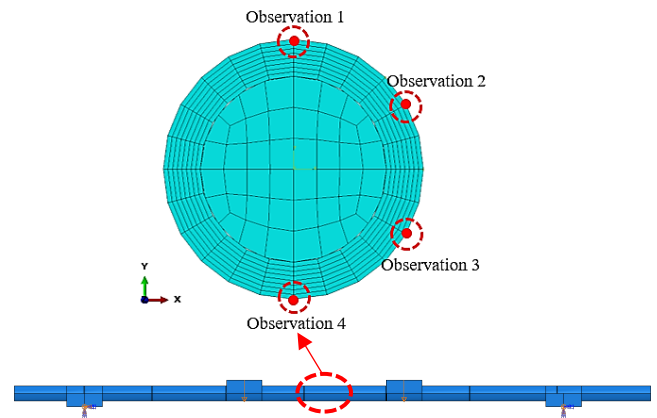
Figure 11 The strain observation position in numerical modeling
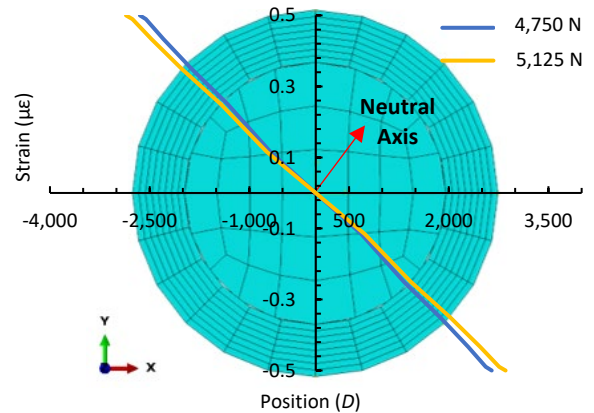
Figure 12 The strain distribution at $P_{elastic}$ and P_{ult} obtained from numerical analysis

This is because 3D modeling still uses material property assumptions following the assumptions used by ISO 22156:2021, namely bamboo as a linear isotropic material.

3.2.2 Strain Distribution

The observation of strain calculated from numerical analysis was conducted at the beam midspan cross-section. The observation was conducted at four nodes, as shown in Figure 11. The nodal

positions depicted in Figure 11 are the same as the strain gauge position attached to the flexural test specimen shown in Figure 2b. Therefore, the strain values obtained from the numerical analysis results are taken from the strain values located in the outer layer of the 4 nodes. They represent the strain on the outer surface of the bamboo. Based on those data,the strain distribution along the beam's cross-section was then created.

The strain distribution when the load reaches the elastic limit (4,750 N) and the ultimate load (5,125 N) can be seen in Figure 12. The figure illustrates that the neutral axis at both step loading is located at the center point of the beam cross-section. However, as depicted in Figure 8, the bending test result shows that the neutral axis is not at the center of the beam cross-section. Moreover, the neutral axis position changes with every change in load. In detail, the differences in the neutral axis position for the elastic limit and ultimate loading step can be seen in Table 4.

Table 4 The difference in neutral axis position between numerical analysis and experimental results

Neutral Axis	Numerical Analysis	Experiment
	Position	Position
$P_{elastic\ limit}$	0	-0.04D
P_{ult}	0	-0.078D

Table 5 The difference in calculation of the total resultant normal force from numerical analysis and theoretical

Load	ΣF_N NA* (kN)	ΣF_N theoretical (kN)	Conclusion
1,000 N	0.002	0	ΣF_N NA* ≈ ΣF_N theoretical
2,000 N	0.003	0	ΣF_N NA* ≈ ΣF_N theoretical
3,000 N	0.004	0	ΣF_N NA* ≈ ΣF_N theoretical
4,000 N	0.006	0	ΣF_N NA* ≈ ΣF_N theoretical
4,750 N	0.006	0	ΣF_N NA* ≈ ΣF_N theoretical
5,125 N	0.007	0	ΣF_N NA* ≈ ΣF_N theoretical

*NA = Numerical Analysis

Table 6 The difference in calculation of the total moment from numerical analysis and theoretical

Load	ΣM NA* (Nmm)	M theoretical (Nmm)	Ratio**
1,000 N	448,452	450,000	0.997
2,000 N	897,488	900,000	0.997
3,000 N	1,346,019	1,350,000	0.997
4,000 N	1,794,469	1,800,000	0.997
4,750 N	2,130,870	2,137,500	0.997
5,125 N	2,299,427	2,306,250	0.997

*NA = Numerical Analysis; **NA/Theoritical

Following up on the difference in neutral axis position between the experiment and the numerical analysis results, validation of the numerical modeling was then carried out. Validation is carried out by calculating the total resultant normal forces F_N and moments M that occurred in the cross-section of the mid-span of the bamboo beam. The calculation is conducted based on the strain distribution obtained from numerical results. Then, the normal force and moment result is compared to that from theoretical calculation. The comparison result of the

normal force and moment can be seen in Table 5 and Table 6, respectively. These two tables show that the numerical analysis result is close to the theoretical calculations result.

Referring to the beam theory, in a laterally loaded beam producing a positive bending moment, normal tensile and compressive stresses occur below and above the neutral axis, respectively. Therefore, the tensile behavior of bamboo parallel to the grain affects the normal tensile stress on the bamboo beam under lateral loading. Like normal tensile stress, the compressive behavior of bamboo parallel to grain affects normal compressive stress.

Previous research shows that the tensile and compressive elastic modulus of bamboo parallel to the grain differs [10,15]. As a result, the neutral axis is not located at the central point of the bamboo cross-section. Thus, the difference in neutral axis position between the experimental and numerical analysis results is caused by using flexural elastic modulus as the mechanical property of bamboo modeling. In other words, bamboo's normal tensile and compressive behavior is assumed to be the same in this bamboo modeling, represented by the flexural elastic modulus.

The strain distribution along the cross-section located in the midspan at the loading step 1,000 N; 2,000 N; 3,000 N; 4,000 N, 4,750 N (elastic limit load); and 5,125 N (ultimate load) can be seen in Figure 13 to Figure 18, respectively. The difference between the strain obtained from the experimental and numerical analysis results can be seen in Table 7 to Table 12. In terms of the maximum compressive strain (at the location of the strain gauge SG-1), the strain ratio of the numerical to the experimental results ranges between 0.85 and 1.02. At the position of the strain gauge SG-2, the strain ratio of the numerical to the experimental results ranges from 0.77 to 1.02.
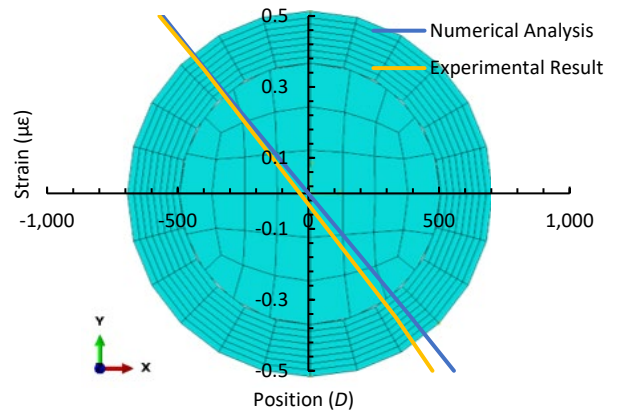
Figure 13 The comparison of strain distribution obtained from experimental and numerical analysis when *P*=1,000 N
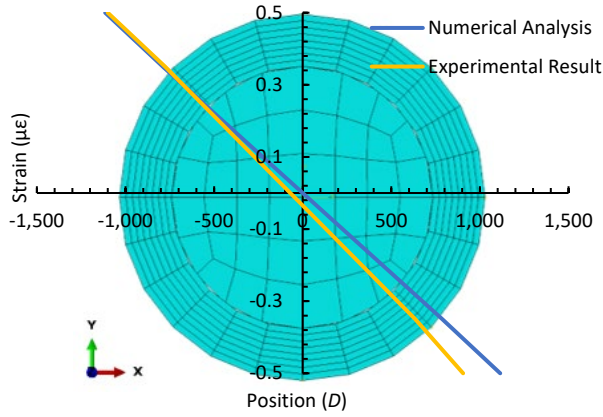
Figure 14 The comparison of strain distribution obtained from experimental and numerical analysis when *P*=2,000 N

Table 7 The strain ratio of SG-1 – SG-4 when *P*=1,000 N

P=1,000 N	Strain (με)		
Position	**Numerical Analysis**	**Experimental**	**Ratio**
	NA	**E**	**NA/E**
0.50*D*	-557	-570	0.98
0.35*D*	-394	-400	0.98
-0.35*D*	394	335	1.18
-0.50*D*	557	475	1.17
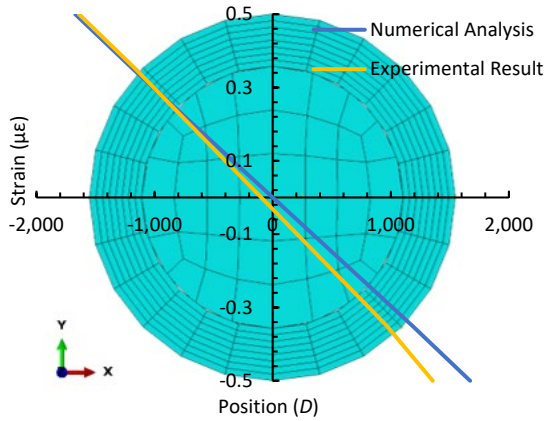
Figure 15 The comparison of strain distribution obtained from experimental and numerical analysis when *P*=3,000 N
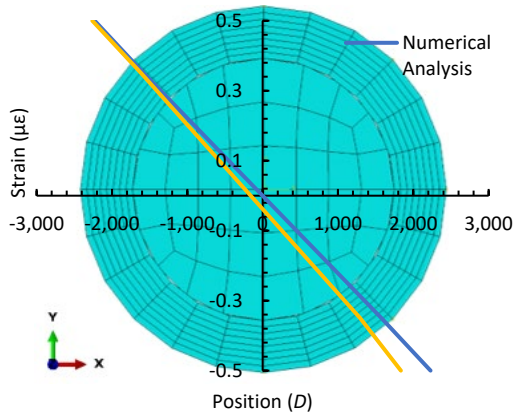
Figure 16 The comparison of strain distribution obtained from experimental and numerical analysis when *P*=4,000 N
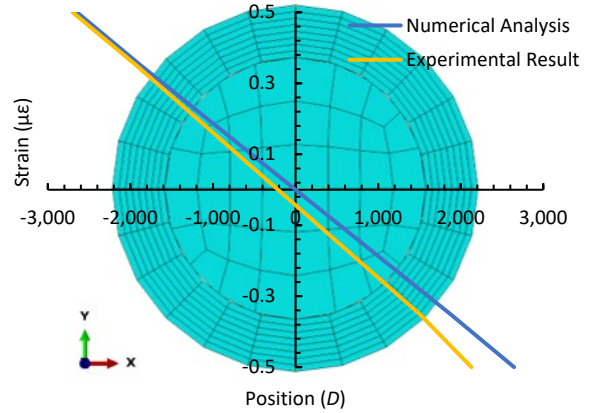
Figure 17 The comparison of strain distribution obtained from experimental and numerical analysis when *P*=4,750 N

At the strain gauge SG-3's position, the numerical to experimental results strain ratio ranges from 1.18 to 1.25. At the position of the strain gauge SG-4, where the maximal normal tensile strain occurs, the strain ratio of the numerical to experimental results ranges from 1.16 to 1.24. The difference between the numerical and experimental results on
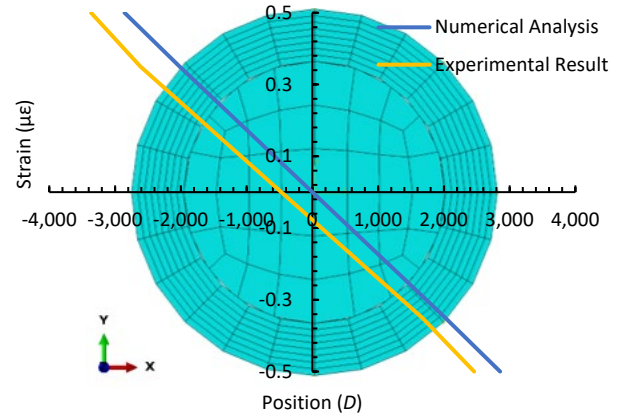
Figure 18 The comparison of strain distribution obtained from experimental and numerical analysis when *P*=5,125 N

Table 8 The strain ratio of SG-1 – SG-4 when *P*=2,000 N

P=2,000 N	Strain (με)		
Position	**Numerical Analysis**	**Experimental**	**Ratio**
	NA	**E**	**NA/E**
0.50*D*	-1,114	-1,100	1.01
0.35*D*	-788	-775	1.02
-0.35*D*	788	635	1.24
-0.50*D*	1,114	905	1.23

Table 9 The strain ratio of SG-1 – SG-4 when *P*=3,000 N

P=3,000 N	Strain (με)		
Position	**Numerical Analysis**	**Experimental**	**Ratio**
	NA	**E**	**NA/E**
0.50*D*	-1,672	-1,640	1.02
0.35*D*	-1,182	-1,160	1.02
-0.35*D*	1,182	965	1.22
-0.50*D*	1,672	1,355	1.23

Table 10 The strain ratio of SG-1 – SG-4 when *P*=4,000 N

P=4,000 N	Strain (με)		
Position	**Numerical Analysis**	**Experimental**	**Ratio**
	NA	**E**	**NA/E**
0.50*D*	-2,229	-2,260	0.99
0.35*D*	-1,576	-1,610	0.98
-0.35*D*	1,576	1,295	1.22
-0.50*D*	2,229	1,835	1.21

compressive strain is lower than that between the numerical and experimental results on tensile strain. Considering this, using the flexural elastic modulus in modeling bamboo beams can predict the maximum compressive strain of the loaded structure well, which ranges from 1.92% to 15.1%. However, this method gives a higher error in predicting the maximum tensile strain of beam structures, ranging from 16.1% to 24.3%.

Table 11 The strain ratio of SG-1 – SG-4 when *P*=4,750 N

P=4,750 N	Strain (με)		
Position	**Numerical Analysis**	**Experimental**	**Ratio**
	NA	**E**	**NA/E**
0.50*D*	-2,647	-2,700	0.98
0.35*D*	-1,871	-1,925	0.97
-0.35*D*	1,872	1,500	1.25
-0.50*D*	2,647	2,130	1.24

Table 12 The strain ratio of SG-1 – SG-4 when *P*=5,125 N

P=5,125 N	Strain (με)		
Position	**Numerical Analysis**	**Experimental**	**Ratio**
	NA	**E**	**NA/E**
0.50*D*	-2,856	-3,365	0.85
0.35*D*	-2,019	-2,615	0.77
-0.35*D*	2,019	1,670	1.21
-0.50*D*	2,855	2,460	1.16

3.2.3 Maximum Normal Stress

The maximum tensile and compressive normal stresses obtained from numerical analysis can be seen in Table 13. The maximum tensile stress is always the same as the compressive stress at each loading step. This is because flexural modulus of elasticity *MoE* is used to determine the mechanical properties of bamboo in numerical modeling. Using flexural modulus of elasticity *MoE* also causes the position of the neutral axis resulting from numerical calculations to always be at half the diameter of the bamboo as previously discussed.

The maximum normal compressive and tensile stresses resulting from numerical calculations, which occur in the cross-section of the mid-span bamboo beam when the bamboo is subjected to the ultimate lateral load, are then compared with the modulus of rupture *MoR* obtained from experiments. Table 13 shows that the maximum normal tensile stress and compressive stress at the ultimate load are each 50.13 MPa. Table 2 shows that the *MoR* value for bamboo from the experiment is 50.4 MPa. The maximum normal stress ratio to *MoR* is 0.995. It means that numerical modeling by assuming that bamboo is a linear isotropic material and using *MoE* as the material properties of the bamboo beam model produces the maximum stress of bamboo at the ultimate load which is almost the same as the *MoR* value.

4.0 CONCLUSION

Based on the results of experimental and the finite element analysis study of Wulung bamboo (*Gigantochloa atroviolacea*), it can be concluded that:

1. The experimental research results show that the flexural modulus of elasticity *MoE* and modulus of rupture *MoR* of Wulung bamboo harvested from Sleman Regency, Yogyakarta Province, Indonesia are 17,562.7 MPa and 50.4 MPa, respectively. The average outer diameter of bamboo is 85.76 MPa. The maximum tensile and compressive strains that occur in the middle span of a bamboo beam loaded with an elastic limit load are 2,130 με and 2,700 με, respectively.

Table 13 Maximum compressive and tensile normal stress of cross-section at the mid-span of the bamboo beam

Load (N)	Compressive Stress (MPa)	Tensile Stress (MPa)
1,000	-9.78	9.78
2,000	-19.56	19.56
3,000	-29.35	29.34
4,000	-39.13	39.13
4,750	-46.46	46.46
5,125	-50.13	50.13

At the same cross-section, the maximum tensile and compressive strains at ultimate loading are 2,460 με and 3,365 με, respectively. The elastic limit load is 4,750 N. The ultimate load is 5,125 N.

2. Observing strain values derived from experimental results is known that the neutral axis is not located in the centroid of the cross-section. It is caused by the difference between the tensile and compressive modulus of elasticity of bamboo parallel to the grain. The neutral axis position changes with every change in load. The neutral axis of the cross-section at the middle span at the elastic limit load is located at -0.04*D*, measured from the center of the cross-section (below the center of the cross-section). When the load is increased to reach the ultimate load, the location of the neutral axis shifts at -0.078*D*.

3. The neutral axis position of the numerical analysis results differs from that of the experimental results. The numerical analysis results that the neutral axis is always located in the center of the cross-section. However, the experiment results

showed that the neutral axis is not located in the centroid of the cross-section. It depends on the tensile and compressive behavior of bamboo parallel to the grain. The difference in neutral axis position is caused by using flexural elastic modulus *MoE* as the mechanical property of bamboo modeling. Using the flexural elastic modulus *MoE* in modeling bamboo beams can predict the maximum compressive strain of the loaded structure, which ranges from 1.92% to 15.1%. This method gives a higher error in predicting the maximum tensile strain of beam structures, ranging from 16.1% to 24.3%.

4. Using the assumption that bamboo is a linear isotropic material, using the bending elastic modulus as a mechanical property of the 3D model, and using the average bamboo diameter from the top and bottom of the bamboo to create a 3D bamboo model results in a load-displacement curve that is close to the load-displacement curve obtained from the experiment. However, the model cannot predict well the load-displacement curve of bamboo beams when the load increases beyond the elastic limit load. Nevertheless, the bamboo beam model can produce the maximum stress of bamboo at the ultimate load which is almost the same as the *MoR* value.

Acknowledgement

We acknowledge the Department of Civil and Environmental Engineering, Engineering Faculty, Universitas Gadjah Mada, for supporting the equipment during the experimental test.

Conflicts of Interest

The author(s) declare(s) that there is no conflict of interest regarding the publication of this paper

References

[1] Abdullah A.H.D., Karlina N., Rahmatiya W., Mudaim S., Patimah, and Fajrin A. R. 2017. Physical And Mechanical Properties Of Five Indonesian Bamboos. *IOP Conference Series: Earth and Environmental Science*. 1-5. DOI: 10.1088/1755-1315/60/1/012014
[2] Ma'Ruf M. F. 2017. A Review on the Use of Bamboo for Earthwork Construction. *MATEC Web Conference, The 6th International Conference of Euro Asia Civil Engineering Forum*. 1-8. DOI: 10.1051/matecconf/201713804010
[3] Tiza T.M., Singh S. K., Kumar L., Shettar M. P., and Singh S. P. 2021. Assessing The Potentials Of Bamboo And Sheep Wool Fiber As Sustainable Construction Materials: A Review. *Material Today Proceeding*. 4484–4489. DOI: 10.1016/j.matpr.2021.05.322.
[4] International Standard Organization ISO-22156. 2021. International Standard Bamboo structures — Bamboo culms — Structural design. Switzerland.
[5] Eratodi I. G. L. B. 2017. Struktur dan Rekayasa Bambu. Denpasar, Bali: Universitas Pendidikan Nasional Denpasar Bali.
[6] Chaowana K., Wisadsatorn S., and Chaowana P. 2021. Bamboo As A Sustainable Building Material—Culm Characteristics And Properties. *Sustainability*.1-18. DOI: https://doi.org/10.3390/su13137376
[7] Akinbade Y., Nettleship I., Papadopoulos C., and Harries K. A. 2021. Modelling Full-Culm Bamboo As A Naturally Varying Functionally Graded Material. *Wood Science Technology*. 155–179. DOI: 10.1007/s00226-020-01246-6.

[8] Oka G. M., Triwiyono A., Awaludin A., and Siswosukarto S. 2014. Effects Of Node, Internode And Height Position On The Mechanical Properties Of Gigantochloa Atroviolacea Bamboo. *Procedia Engineering, 2nd International Conference on Sustainable Civil Engineering Structures and Construction Materials*. 31-37. DOI: 10.1016/j.proeng.2014.12.162.
[9] Candelaria M. D. E. and Hernandez J. Y. 2019. Determination of the Properties of Bambusa Blumeana Using Full-Culm Compression Tests and Layered Tensile Tests for Finite Element Model Simulation Using Orthotropic Material Modeling. *ASEAN Engineering Journal*. 54–71. DOI: 10.11113/aej.v9.15508.
[10] Suriani E. 2020. A Study of the Physical-Mechanical Properties of Bamboo in Indonesia. *Proceedings of the Built Environment, Science and Technology International Conference*. 154–162. DOI: 10.5220/0008904601540162.
[11] Siopongco M., J.O.; Munandar. 1987. Technology Manual On Bamboo As Building Material. *Forest Products Research and Development Institute*.
[12] Sato M., Inoue A., and Shima H. 2017. Bamboo-Inspired Optimal Design For Functionally Graded Hollow Cylinders. *PLoS ONE*. 1–14. DOI: https://doi.org/10.1371/journal.pone.0175029
[13] Tan T. et al. 2011. Mechanical Properties Of Functionally Graded Hierarchical Bamboo Structures. *Acta Biomaterial*. 3796–3803. DOI: 10.1016/j.actbio.2011.06.008.
[14] Irawati I. S. and Wusqo U. 2020. Perbandingan Perilaku Lentur Balok Bambu Menggunakan Sifat Mekanik yang Diperoleh dengan Metode Rata-rata dan Persentil ke-5. *Jurnal Permukiman*. 1–23. DOI: https://doi.org/10.31815/jp.2020.15.43-53
[15] Ramful R. and Sakuma A. 2020. Investigation Of The Effect Of Inhomogeneous Material On The Fracture Mechanisms Of Bamboo By Finite Element Method. *Materials (Basel)*. 1–15 DOI: 10.3390/ma13215039.
[16] Abzarih A. W., Irawati I. S., and Suhendro B. 2022. Nonlinear Numerical Model of Glued-Laminated Petung Bamboo Under Flexural Test Based on ASTM D 143-94. *Proceeding 5th International Conference Sustainable Civil Engineering Structures Construction Material*. DOI: 10.1007/978-981-16-7924-7.
[17] Junaid A., Irawati I. S., and Awaludin A. 2022. Analisis Sifat Mekanis dan Fisis Bambu Menggunakan Metode Destruktif. *Jurnal Teknik Sipil MACCA*. 41–49. DOI: https://doi.org/10.33096/jtsm.v7i1.540
[18] Nurmadina, Nugroho N., and Bahtiar E. T. 2017. Structural Grading Of Gigantochloa Apus Bamboo Based On Its Flexural Properties. *Construction Building Material*. 1173–1189. DOI: 10.1016/j.conbuildmat.2017.09.170.
[19] Bahtiar E. T., Imanullah A. P., Hermawan D., Nugroho N., and Abdurachman. 2019. Structural grading of three sympodial bamboo culms (Hitam, Andong, and Tali) subjected to axial compressive load. *Engineering Structures*. 233-245. DOI: 10.1016/j.engstruct.2018.12.026.
[20] Firdaus A., Prastyatama B., Sagara A., and Wirabuana R. N. 2017. Deployable bamboo structure project: A building life-cycle report. *AIP Conference Proceeding*. 1-7. DOI: 10.1063/1.5011509.
[21] Fitrianto A. 2015. Bamboo architecture for sustainable communities. *Parahyangan Bamboo Nation 2*. 1-8.
[22] Awaludin A. and Andriani V. 2014. Bolted bamboo joints reinforced with fibers. *Proceeding 5th International Conference Sustainable Civil Engineering Structures Construction Material*. 15–21. DOI: 10.1016/j.proeng.2014.12.160.
[23] Taufani A. R. and Nugroho A. S. B. 2014. Proposed bamboo school buildings for elementary schools in Indonesia. *Proceeding 5th International Conference Sustainable Civil Engineering Structures Construction Material*.5–14. DOI: 10.1016/j.proeng.2014.12.159.
[24] International Standard Organization ISO-22157. 2019. International Standard Bamboo structures — Determination of physical and mechanical properties. Switzerland
[25] Willam KJ. 2002. Constitutive Models For Engineering Materials. *Encyclopedia of Physical Science and Technology*. 603–633.
[26] Shames I. H. 2020. Linear Elastic Behavior Elastic And Inelastic Stress Analysis. 147–176. DOI: 10.1201/b16599-8
[27] Li H. T., Deeks A. J., Zhang Q. S., and Wu G. 2016. Flexural Performance Of Laminated Bamboo Lumber Beams. *BioResources*. 929–943. DOI: 10.15376/biores.11.1.929-943.